Received: 7 July 2022 | Revised: 18 October 2022 | Accepted: 21 October 2022

DOI: 10.1002/nme.7149

RESEARCH ARTICLE

WILEY

Superconvergence of the effective Cauchy stress in computational homogenization of inelastic materials

Matti Schneider | **Daniel Wicht**

Institute of Engineering Mechanics, Karlsruhe Institute of Technology (KIT), Karlsruhe, Germany

Correspondence
Matti Schneider, Institute of Engineering Mechanics, Karlsruhe Institute of Technology (KIT), Karlsruhe, Germany.
Email: matti.schneider@kit.edu

Funding information
Deutsche Forschungsgemeinschaft, Grant/Award Number: 255730231;
European Research Council, Grant/Award Number: 101040238

Abstract

We provide theoretical investigations and empirical evidence that the effective stresses in computational homogenization of inelastic materials converge with a higher rate than the local solution fields. Due to the complexity of industrial-scale microstructures, computational homogenization methods often utilize a rather crude approximation of the microstructure, favoring regular grids over accurate boundary representations. As the accuracy of such an approach has been under continuous verification for decades, it appears astonishing that this strategy is successful in homogenization, but is seldom used on component scale. A part of the puzzle has been solved recently, as it was shown that the effective elastic properties converge with twice the rate of the local strain and stress fields. Thus, although the local mechanical fields may be inaccurate, the averaging process leads to a cancellation of errors and improves the accuracy of the effective properties significantly. Unfortunately, the original argument is based on energetic considerations. The straightforward extension to the inelastic setting provides superconvergence of (pseudoelastic) potentials, but does not cover the primary quantity of interest: the effective stress tensor. The purpose of the work at hand is twofold. On the one hand, we provide extensive numerical experiments on the convergence rate of local and effective quantities for computational homogenization methods based on the fast Fourier transform. These indicate the superconvergence effect to be valid for effective stresses, as well. Moreover, we provide theoretical justification for such a superconvergence based on an argument that avoids energetic reasoning.

KEYWORDS

computational homogenization, effective properties, FFT-based computational micromechanics, Galerkin discretization, superconvergence

1 | INTRODUCTION

1.1 | State of the art

Computational micromechanics[1] has been firmly established as a link between material models of the constituent phases and the effective material behavior of microheterogeneous materials, in particular for rather complex material

behavior and industrial-scale microstructures, see Matouš et al.[2] for an overview. Modern computational homogenization methods need to account for these challenges, in particular involving the mesh generation for microstructures, for example, provided from digital volume-image techniques, and the rather high stresses emerging on the microscopic scale.

Methods tailored to regular grids[3-6] turned out to be quite successful, as they avoid the meshing procedure altogether and because the discretization on a regular grid enables code optimizations[7-9] unavailable for heterogeneous meshes. Yet, at second glance, their success comes with an element of surprise, as the accuracy of the local fields is well-known to be suboptimal. Still, such methods have been around for at least 25 years, and have been subject to a number of critical assessments.[10-12]

Within the community, it has been known that the computed effective properties can oftentimes be trusted despite a lacking fidelity in the local solution fields. For instance, Schneider et al.[13], section 4.1.2, state that "*the error (of the effective stresses) decreases linearly with the grid spacing (…) This superconvergence behavior is quite surprising, as the local error* $\|u - u_h\|_{H^1}$ *is only of order* $h^{1/2}$ *for voxel-FEM*." Only recently, this superconvergence of the effective stresses has been investigated from a theoretical point of view. Ye-Chung[14] showed that, for a general microstructure, the effective elastic properties converge with twice the rate of the local strain field in the L^2-norm. A related statement had been proved earlier for the iteration error by Bellis et al.[15] In fact, the techniques used by Bellis et al.[15] could be used to improve the result of Ye-Chung[14] to show that, for a general microstructure, the effective (free) energy of a (small-strain) hyperelastic composite material converges with twice the L^2-rate of the local strain field, provided the (free) energy has a Lipschitz-continuous gradient.

These results provide the theoretical underpinnings for the unreasonable effectiveness of voxel-based methods in computational homogenization. Indeed, despite their rather crude approximation of the microstructure geometry, the effective properties may be computed with reasonable accuracy. Indeed, suppose for a moment that, instead of the familiar convergence proportional to h, the voxel edge-length, the effective properties would converge with $h^{1/2}$. Then, roughly speaking, decreasing the error in the effective properties by a factor of two would require to consider $64 = 8^2$ times as many degrees of freedom in three spatial dimensions. Instead, an h-convergence dictates that considering eight times as many degrees of freedom is sufficient to decrease the error by a factor of two.

As stated in the beginning, computational micromechanics has evolved rapidly in the last two decades, and rather complex inelastic constitutive models may be treated on long time scales.[16-18] Thus, there is an immediate interest whether the confidence in regular-grid-based homogenization methods is justified when inelastic materials are considered. Mathematically speaking, this entails the question of superconvergence of the effective stresses under inelastic homogenization and computationally feasible approximations. Yet, the existing theoretical arguments[14,15] are based on an energetic reasoning. In particular, they provide a superconvergence result for the (free) energy, but their argument does not readily permit to draw conclusions about the effective stress, that is, the partial derivative of the effective (free) energy w.r.t. the macroscopic strain tensor. Only in the context of linear elasticity, where the (free) energy is quadratic, results for the effective stress may be extracted readily.

1.2 | Contributions

The article at hand investigates two research questions, which are of independent interest but whose joint treatment comes with synergy effects. As pointed out earlier, there is a variety of works investigating discretization schemes and convergence rates for linear computational homogenization problems. However, thorough computational investigations on the accuracy of discretizations and convergence rates of both effective and local quantities is lacking for inelastic homogenization in solid mechanics. This defect is completely reasonable, because there is a significant effort involved in such studies, in particular when sufficiently converged reference quantities are desired. The work at hand provides such benchmarks for state-of-the-art computational methods based on the fast Fourier transform (FFT), including quasi-static computational experiments for polymers with glass reinforcements, a metal-matrix composite and a polycrystalline microstructure, see Section 3. The computational results show empirically that the local stress and strain fields converge, in the L^2-norm, with a rate $h^{1/2}$ in the voxel edge-length h, whereas the Cauchy stress converges (at least) with an order h. Thus, there is reason to expect the effective Cauchy stress to converge with a higher rate when homogenizing certain classes of inelastic materials, as well.

Independent of the computational investigations, we investigate the convergence behavior of the effective stresses from a theoretical point of view. Restricted to an isothermal, small-strain and quasi-static framework, we uncover the

basic mechanisms responsible for the superconvergence behavior of the effective stresses in a Galerkin setting and with an implicit time discretization of inelastic problems in mind. We present a number of assumptions in Section 2.1 which are sufficient to derive superconvergence results. Before discussing those assumptions further, we wish to comment on the proof technique, as it is interesting in itself. Instead of the (free) energy, we consider the mechanical work as the bilinear quantity of interest. Indeed, the arguments of Bellis et al.[15] could be used to show a superconvergence behavior of the effective (incremental) energy, but we are not aware of a corresponding result for the effective Cauchy stress, that is, the derivative of the effective energy.

On second thought, considering the mechanical work is quite natural in view of the Hill–Mandel condition.[19,20] Working in a time discretization permits us to instead consider inner products between local strain and stress fields, not necessarily related by the constitutive law, and their macroscopic equivalents. As the stress field satisfies the balance equation, we are free to choose the local strain "test field" as desired. From the theoretical arguments it becomes apparent that choosing the *tangent corrector* is most convenient in this setting, see Section 2.2.

We consider two classes of assumptions. The first category works with minimal assumptions on the constitutive law, but permits to conclude only superconvergence per se, that is, improving the big-O convergence rate of the local stresses to a small-o convergence rate of the effective stresses. Moreover, we consider more restrictive assumptions, that is, Lipschitz continuity of the algorithmic tangent and boundedness of the linearized corrector, which are rather restrictive, but permit us to double the convergence rate of the local stress field upon averaging.

Although we started our argument with the computational experiments, we decided to discuss the theoretical developments first in order to maintain a smoother reading experience for the reader.

Some caution has to be taken, as the computational experiments should not be considered as a validation of the theoretical arguments or as an investigation of their sharpness. Indeed, there are certain discrepancies that we will briefly discuss. For a start, fully integrated finite elements on regular grids can be handled by FFT-based methods,[21-23] but do not give rise to the best compromise between accuracy and computational effort. Indeed, fully integrated elements require either a higher computational effort or an increased memory footprint, and computational experiments suggest their accuracy is not superior compared to more traditional discretizations (Reference 24, section 1.2). Thus, we decided to investigate the most popular discretizations employed in FFT-based methods instead. Moreover, we did not focus on which materials satisfy the assumptions required by the theory. Rather, we investigate material models of broad practical interest, where an empirical confirmation of superconvergence properties is also of interest.

Thus, there is a significant gap between the theoretical results—which cover a Galerkin setting and strongly monotone material models whose solutions enjoy judicious regularity properties—and the computational experiments, where full integration is usually avoided and the material models may not satisfy the requirements for the theory to hold. Closing this gap requires further ideas.

Last but not least we wish to discuss the connection to superconvergence of finite element methods, a subject with a long history. In this context, the order of convergence of finite element approximations of partial differential equations may be improved via postprocessing. Typically, *local* techniques may be used, which employ weighted averages of the finite element solution at special points, for example, via edge averages[25,26] or nodal averages,[27,28] see also Babuška et al.[29,30] for more background. Alternatively, *global* postprocessing techniques are based on solving an additional finite element problem, which may be used to improve the accuracy significantly but comes at a low computational expense. Such global approaches may, for instance, utilize different resolutions in time[31-33] or space.[34-36]

The approach considered in this article is different in spirit, as no additional computations are necessary. Rather, the ideas underlying the described techniques may be used for theoretical convergence analysis. Indeed, for a fixed solution to the nonlinear or inelastic unit-cell problem we use the solution to an auxiliary problem to show an improved convergence behavior of the effective, that is, averaged, stresses. Actually, for each individual component of the effective Cauchy stress tensor (six independent ones in three spatial dimensions) an auxiliary field is used based on solving the linearized corrector equation. In this way, an bilinear quantity is set up as the basis for the improved convergence analysis.

Another difference is that the problems we consider are highly heterogeneous, whereas the convergence improvement techniques discussed earlier are typically restricted to homogeneous problems. For the problem at hand, the linearized corrector equation should be thought of as a natural "filter" weighting the local stress field in an advantageous way. This phenomenon may also be used to postprocess inaccurate solutions to increase their accuracy, see Schneider[37] for the linear elastic case.

2 | THEORETICAL CONSIDERATIONS

2.1 | Background and assumptions

We are concerned with a rectangular unit cell

$$Q = [0, L_1] \times [0, L_2] \times \cdots \times [0, L_d], \tag{1}$$

in d dimensions and we suppose that a nonlinear elastic stress function

$$\mathcal{A} : Q \times \mathrm{Sym}(d) \to \mathrm{Sym}(d) \tag{2}$$

is given, where $\mathrm{Sym}(d)$ denotes the space of symmetric $d \times d$-tensors. At every continuum point $x \in Q$ and for every strain $\varepsilon \in \mathrm{Sym}(d)$, the quantity $\mathcal{A}(x, \varepsilon)$ provides the current stress at point x for prescribed strain ε. The setting (2) includes inelastic materials when considering an incremental framework in a quasi-static setting, that is, statically condensing the internal variables for a fixed time step, see Ortiz-Stainier[38] or Miehe.[39]

For the succeeding arguments, we impose the following restrictions[40] on the local stress operator (2):

1. The field $\mathcal{A}(\cdot, 0)$ is essentially bounded, that is, $\mathcal{A}(\cdot, 0) \in L^\infty(Q; \mathrm{Sym}(d))$.
2. For any strain $\varepsilon \in \mathrm{Sym}(d)$, the field $\mathcal{A}(\cdot, \varepsilon)$ is measurable.
3. There is a constant $\alpha_+ > 0$, s.t. the Lipschitz condition

$$\|\mathcal{A}(x, \varepsilon_1) - \mathcal{A}(x, \varepsilon_2)\| \leq \alpha_+ \, \|\varepsilon_1 - \varepsilon_2\|, \tag{3}$$

   holds for all $\varepsilon_1, \varepsilon_2 \in \mathrm{Sym}(d)$ and almost every $x \in Q$.
4. There is a constant $\alpha_- > 0$, s.t. the strong monotonicity condition

$$(\mathcal{A}(x, \varepsilon_1) - \mathcal{A}(x, \varepsilon_2)) : (\varepsilon_1 - \varepsilon_2) \geq \alpha_- \, \|\varepsilon_1 - \varepsilon_2\|^2, \tag{4}$$

   holds for all $\varepsilon_1, \varepsilon_2 \in \mathrm{Sym}(d)$ and almost every $x \in Q$.
5. For almost any x, the function $\mathrm{Sym}(d) \ni \varepsilon \mapsto \mathcal{A}(x, \varepsilon)$ is continuously differentiable. We denote the derivative, that is, the *algorithmic tangent* in an incremental pseudo-elastic setting,[38,39] by

$$\mathbb{A}(x, \varepsilon) \equiv \frac{\partial \mathcal{A}}{\partial \varepsilon}(x, \varepsilon), \quad x \in Q, \quad \varepsilon \in \mathrm{Sym}(d). \tag{5}$$

   For the improved convergence estimate, it is moreover required that the algorithmic tangent is Lipschitz continuous, that is, there is a constant $M > 0$, s.t. the estimate

$$\|\mathbb{A}(x, \varepsilon_1) - \mathbb{A}(x, \varepsilon_2)\| \leq M \, \|\varepsilon_1 - \varepsilon_2\|, \quad x \in Q, \quad \varepsilon_1, \varepsilon_2 \in \mathrm{Sym}(d), \tag{6}$$

   holds.

For the inequalities (3) and (4), we use the Frobenius norm

$$\|\varepsilon\| \equiv \sqrt{\varepsilon : \varepsilon} \equiv \sqrt{\sum_{i,j=1}^{d} \varepsilon_{ij}^2}, \quad \varepsilon \in \mathrm{Sym}(d), \tag{7}$$

and the Frobenius inner product

$$\varepsilon : \xi \equiv \sum_{i,j=1}^{d} \varepsilon_{ij} \xi_{ij}, \quad \varepsilon, \xi \in \mathrm{Sym}(d). \tag{8}$$

The norm in the left-hand side of inequality (6) refers to the induced operator norm, that is,

$$\|\mathbb{L}\| := \sup\left\{ \|\mathbb{L} : \varepsilon\| \;\middle|\; \varepsilon \in \mathrm{Sym}(d) \quad \text{with} \quad \|\varepsilon\| \leq 1 \right\}, \tag{9}$$

for any linear operator $\mathbb{L}$ on $\mathrm{Sym}(d)$ and where the norm in brackets refers to the Frobenius norm (7). Actually, the monotonicity condition (4) can be significantly weakened to include porous materials of practical interest, see Schneider.[40] To avoid some of the inherent technicalities, we restrict to the coercive setting (4). Let us record for later use that continuous differentiability statement for the operator $\varepsilon \mapsto \mathcal{A}(x,\varepsilon)$, a part of assumption 5., implies the identity

$$\mathcal{A}(x,\xi) - \mathcal{A}(x,\varepsilon) = \int_0^1 \mathbb{A}(x,\varepsilon + s(\xi-\varepsilon)) : (\xi-\varepsilon)\, ds \equiv \int_0^1 \mathbb{A}(x,\varepsilon + s(\xi-\varepsilon))\, ds : (\xi-\varepsilon), \tag{10}$$

as a direct consequence of the fundamental theorem of calculus. The conditions 1–3. ensure that the constitute law (2) may be extended viz-a-viz to a well-defined operator on Lebesgue spaces, the so-called Nemytskii operator (Reference 41, section 10.3.4),

$$\sigma : L^2(Q;\mathrm{Sym}(d)) \to L^2(Q;\mathrm{Sym}(d)), \quad \varepsilon \mapsto \mathcal{A}(\cdot,\varepsilon(\cdot)). \tag{11}$$

The condition (3) implies that the stress operator is Lipschitz continuous

$$\|\sigma(\varepsilon_1) - \sigma(\varepsilon_2)\|_{L^2} \leq \alpha_+ \, \|\varepsilon_1 - \varepsilon_2\|_{L^2}, \quad \varepsilon_1, \varepsilon_2 \in L^2(Q;\mathrm{Sym}(d)), \tag{12}$$

whereas condition (4) ensures a strong monotonicity condition

$$(\sigma(\varepsilon_1) - \sigma(\varepsilon_2), \varepsilon_1 - \varepsilon_2)_{L^2} \geq \alpha_- \, \|\varepsilon_1 - \varepsilon_2\|_{L^2}^2, \quad \varepsilon_1, \varepsilon_2 \in L^2(Q;\mathrm{Sym}(d)), \tag{13}$$

for the Frobenius-based L^2-inner product

$$(\varepsilon, \xi)_{L^2} = \langle \varepsilon : \xi \rangle_Q, \quad \varepsilon, \xi \in L^2(Q;\mathrm{Sym}(d)), \tag{14}$$

and the averaging integral

$$\langle f \rangle_Q = \frac{1}{L_1 \cdots L_d} \int_Q f(x)\, dx, \quad f \in L^1(Q). \tag{15}$$

In (periodic) homogenization at small strains and in a quasi-static framework, for prescribed macroscopic strain $\overline{\varepsilon}$ we are concerned with finding a solution $u \in H^1_\#(Q;\mathbb{R}^d)$ to the corrector equation

$$\mathrm{div}\ \ \sigma(\overline{\varepsilon} + \nabla^s u) = 0, \tag{16}$$

where $H^1_\#(Q;\mathbb{R}^d)$ is the H^1-closure of mean-free fields which are Q-periodic together with their first derivatives, and the symmetrized gradient operator

$$\nabla^s : H^1_\#(Q;\mathbb{R}^d) \to L^2(Q;\mathrm{Sym}(d)), \tag{17}$$

as well as its negative adjoint

$$\mathrm{div} \ \ : L^2(Q;\mathrm{Sym}(d)) \to H^{-1}_\#(Q;\mathbb{R}^d) \equiv \left(H^1_\#(Q;\mathbb{R}^d)\right)', \tag{18}$$

both extending the corresponding differential operators defined on smooth fields. In a finite-element framework, it is often more convenient to rewrite Equation (16) in a weak form

$$\left\langle \nabla^s w : \sigma(\overline{\varepsilon} + \nabla^s u) \right\rangle_Q = 0 \quad \text{for all} \quad w \in H^1_\#(Q;\mathbb{R}^d), \tag{19}$$

using integration by parts. Under the assumptions, in particular the inequalities (12) and (13), it is straightforward to show existence and uniqueness of a solution u to the corrector equation (16). With this solution at hand, the effective stress $\overline{\sigma}(\overline{\varepsilon})$ response, the primary quantity of interest, may be computed via

$$\overline{\sigma}(\overline{\varepsilon}) = \left\langle \sigma(\overline{\varepsilon} + \nabla^s u) \right\rangle_Q , \tag{20}$$

as the spatial average of the local stress field.

With obtaining computable approximations to the effective stress in mind, (conforming) Galerkin methods select a closed subspace $V_h \subseteq H^1_\#(Q;\mathbb{R}^d)$, typically corresponding to linear combinations of ansatz functions, and seek a solution $u_h \in V_h$ subject to the condition

$$\left\langle \nabla^s w_h \,:\, \sigma(\overline{\varepsilon} + \nabla^s u_h) \right\rangle_Q = 0 \quad \text{for all} \quad w_h \in V_h, \tag{21}$$

which approximates the continuous condition (19). Due to the subspace property, the monotonicity and Lipschitz continuity properties are inherited, and existence and uniqueness of a solution u_h to equation (21) is immediate. In a Galerkin framework, and under the conditions (12) and (13), the a priori estimate

$$\|\nabla^s u - \nabla^s u_h\|_{L^2} \leq \frac{\alpha_+}{\alpha_-} \, \|\nabla^s u - \nabla^s w_h\|_{L^2}, \tag{22}$$

holds for all $w_h \in V_h$. In particular, one may select the best approximation $w_h = P_h w$ with the orthogonal projector

$$P_h \,:\, H^1_\#(Q;\mathbb{R}^d) \to V_h, \quad P_h u = \arg\min_{w_h \in V_h} \|\nabla^s u - \nabla^s w_h\|_{L^2}, \tag{23}$$

to obtain the bound

$$\|u - u_h\|_{H^1_0} \leq \frac{\alpha_+}{\alpha_-} \, \|u - P_h u\|_{H^1_0}, \tag{24}$$

involving the inner product

$$(u,v)_{H^1_0} \equiv \langle \nabla^s u \,:\, \nabla^s v \rangle_Q , \quad u, v \in H^1_\#(Q;\mathbb{R}^d). \tag{25}$$

Let us emphasize again that the effective stress (20) is the basic quantity of interest in (nonlinear) homogenization which is approximated by

$$\overline{\sigma}_h(\overline{\varepsilon}) = \left\langle \sigma(\overline{\varepsilon} + \nabla^s u_h) \right\rangle_Q , \tag{26}$$

where $u_h \in V_h$ solves Equation (21). With the representation

$$\overline{\sigma} - \overline{\sigma}_h = \left\langle \sigma(\overline{\varepsilon} + \nabla^s u) - \sigma(\overline{\varepsilon} + \nabla^s u_h) \right\rangle_Q , \tag{27}$$

it is elementary to estimate

$$\begin{aligned} \left\| \overline{\sigma} - \overline{\sigma}_h \right\| &\leq \left\| \sigma(\overline{\varepsilon} + \nabla^s u) - \sigma(\overline{\varepsilon} + \nabla^s u_h) \right\|_{L^2} \\ &\leq \alpha_+ \, \|\nabla^s u - \nabla^s u_h\|_{L^2} \\ &\leq \tfrac{\alpha_+^2}{\alpha_-} \, \|u - P_h u\|_{H^1_0} , \end{aligned} \tag{28}$$

where we used the Lipschitz continuity (12) and the a priori estimate (24). Thus, the bound (28) shows that the effective stresses converge at least as fast as the H^1_0-norm of the local displacement field. Put differently, if the regularity of the solution u and the used Galerkin space V_h leads to a convergence behavior

$$\|u - P_h u\|_{H^1_0} = O(h^p), \tag{29}$$

for a power $p > 0$, the estimate (28) entails

$$\left\| \overline{\sigma}(\overline{\varepsilon}) - \overline{\sigma}_h(\overline{\varepsilon}) \right\| = O(h^p). \tag{30}$$

Please note that, for general microstructures, and discontinuous coefficients, $p = 1/2$ is the highest power expected in the estimate (29) for finite elements on a regular grid, independent of the order of the finite elements. This is readily seen by examining, for instance, a two-phase laminate. Moreover, Ye-Chung[14] show that the estimate (29) holds for $p = 1/2$ under specific assumptions on the stiffness distribution. More precisely, they critically rely on the Li-Nirenberg[42] estimates which show that the local strain field solving the corrector equation (21) is essentially bounded provided the stiffness distribution is sufficiently smooth on a tessellation of the microstructure, and the interfaces between the individual tiles (or "phases") is smooth enough. In particular the latter condition is rather restrictive for practical materials. For instance, fiber-reinforced materials which model the fibers as cylinders lead to non-smooth interfaces, as do the grains in a Voronoi or Laguerre tessellation. For such problems, estimates in weighted spaces may be useful, see Mazzucato-Nistor[43] and references therein.

The starting point of this article was the fact that if the constitutive law $\mathcal{A}$ is linear, that is, Hooke's law

$$\mathcal{A}(x, \varepsilon) = \mathbb{C}(x) : \varepsilon, \quad x \in Q, \quad \varepsilon \in \mathrm{Sym}(d), \tag{31}$$

is valid in terms of a suitable heterogeneous field of stiffness tensors $\mathbb{C}$, the estimate

$$\left\| \overline{\sigma}(\overline{\varepsilon}) - \overline{\sigma}_h(\overline{\varepsilon}) \right\| = O(h^{2p}), \tag{32}$$

holds, see Ye-Chung,[14] theorem 5. In particular, the effective stresses converge with twice the rate as the local fields. A natural question emerges whether a similar superconvergence result is also valid for more general constitutive laws than linear elasticity (31).

2.2 | Superconvergence of effective stresses

For the following considerations, we suppose that the macroscopic strain $\overline{\varepsilon} \in \mathrm{Sym}(d)$ is fixed, together with the solutions $u \in H^1_{\#}(Q; \mathbb{R}^d)$ and $u_h \in V_h$ of Equations (19) and (21), respectively. To keep the notation concise, we introduce the fields

$$\varepsilon = \overline{\varepsilon} + \nabla^s u \in L^2(Q; \mathrm{Sym}(d)) \quad \text{and} \quad \varepsilon_h = \overline{\varepsilon} + \nabla^s u_h \in L^2(Q; \mathrm{Sym}(d)). \tag{33}$$

For fixed $\overline{\xi} \in \mathrm{Sym}(d)$, we make use of the (transposed) linearized corrector $v \in H^1_{\#}(Q; \mathbb{R}^d)$ which solves the equation

$$\left\langle \nabla^s w : \mathbb{A}(\cdot, \varepsilon)^T : (\overline{\xi} + \nabla^s v) \right\rangle_Q = 0 \quad \text{for all} \quad w \in H^1_{\#}(Q; \mathbb{R}^d). \tag{34}$$

Here, transposition refers to major transposition, that is,

$$\left(\mathbb{A}(x, \varepsilon)^T\right)_{ijkl} = (\mathbb{A}(x, \varepsilon))_{klij}, \quad x \in Q, \quad \varepsilon \in \mathrm{Sym}(d), \tag{35}$$

in component notation. It is immediate to see that the field $\mathbb{A}(\cdot, \varepsilon)^T$ is α_--strongly monotone and α_+-Lipschitz continuous, implying the existence and uniqueness of a solution to Equation (34). Let us write

$$\xi = \overline{\xi} + \nabla^s v \in L^2(Q; \mathrm{Sym}(d)) \quad \text{and} \quad \xi_h = \overline{\xi} + \nabla^s v_h \in L^2(Q; \mathrm{Sym}(d)) \quad \text{for} \quad v_h = P_h v. \tag{36}$$

Let us investigate the quantity

$$\langle (\xi - \xi_h) : (\sigma(\varepsilon) - \sigma(\varepsilon_h)) \rangle_Q = \langle (\xi - \xi_h) : \sigma(\varepsilon) \rangle_Q - \langle (\xi - \xi_h) : \sigma(\varepsilon_h) \rangle_Q . \tag{37}$$

By the corrector equation (16), the first term

$$\langle (\xi - \xi_h) : \sigma(\varepsilon) \rangle_Q \equiv \langle \nabla^s (v - v_h) : \sigma(\varepsilon) \rangle_Q = 0, \tag{38}$$

vanishes. Thus, we may write

$$\begin{aligned} \langle (\xi - \xi_h) : (\sigma(\varepsilon) - \sigma(\varepsilon_h)) \rangle_Q &= - \langle (\xi - \xi_h) : \sigma(\varepsilon_h) \rangle_Q \\ &= \langle \xi_h : \sigma(\varepsilon_h) \rangle_Q - \langle \xi : \sigma(\varepsilon_h) \rangle_Q \\ &= \langle \xi_h : \sigma(\varepsilon_h) \rangle_Q - \langle \xi : \sigma(\varepsilon) \rangle_Q + \langle \xi : (\sigma(\varepsilon) - \sigma(\varepsilon_h)) \rangle_Q , \end{aligned} \tag{39}$$

where we added a zero for our convenience. Using the balance equations (19) and (21), respectively, we notice

$$\langle \xi : \sigma(\varepsilon)\rangle_Q = \left\langle \overline{\xi} : \sigma(\varepsilon)\right\rangle_Q + \langle \nabla^s v : \sigma(\varepsilon)\rangle_Q = \overline{\xi} : \overline{\sigma}(\overline{\varepsilon}), \tag{40}$$

and

$$\langle \xi_h : \sigma(\varepsilon_h)\rangle_Q = \left\langle \overline{\xi} : \sigma(\varepsilon_h)\right\rangle_Q + \langle \nabla^s v_h : \sigma(\varepsilon_h)\rangle_Q = \overline{\xi} : \overline{\sigma}_h(\overline{\varepsilon}). \tag{41}$$

We thus obtain an expression for the $\overline{\xi}$-component of the difference in the effective stresses (20) and (26)

$$\overline{\xi} : \overline{\sigma}_h(\overline{\varepsilon}) - \overline{\xi} : \overline{\sigma}(\overline{\varepsilon}) = \langle (\xi - \xi_h) : (\sigma(\varepsilon) - \sigma(\varepsilon_h))\rangle_Q + \langle \xi : (\sigma(\varepsilon) - \sigma(\varepsilon_h))\rangle_Q . \tag{42}$$

We have just derived the most fundamental formula of the paper at hand. It expresses the difference between the effective stress and its Galerkin approximation in the strain direction $\overline{\xi}$ exactly in terms of a quadratic expression involving the differences in stresses and strain directions as well as a linear term in the stress difference. Let us remark at this point that the representation (42) of the error is *exact*. To proceed, some estimates are necessary, which may or may not be sharp, and which require suitable assumptions. To be more precise, we consider two classes of assumptions. We will start with minimal assumptions which are typically satisfied, but lead to rather conservative conclusions. Then, we will consider more restrictive assumptions, which are hard to verify for practical materials, but which allow us to draw rather strong conclusions.

We will start with the minimal assumptions, as introduced in the previous section. The fundamental Theorem of calculus (10) serves as our departure, s.t. we may write

$$\sigma(\varepsilon_h) - \sigma(\varepsilon) = \int_0^1 \mathbb{A}(\cdot, \varepsilon + s(\varepsilon_h - \varepsilon)) : (\varepsilon_h - \varepsilon)\, ds. \tag{43}$$

As the field ξ was selected to solve the linearized problem (34), we obtain the expression

$$0 = \left\langle \nabla^s(u_h - u) : \mathbb{A}(\cdot, \varepsilon)^T : \xi\right\rangle_Q = \left\langle \varepsilon_h - \varepsilon : \mathbb{A}(\cdot, \varepsilon)^T : \xi\right\rangle_Q = \langle \xi : \mathbb{A}(\cdot, \varepsilon) : (\varepsilon_h - \varepsilon)\rangle_Q . \tag{44}$$

Inserting this equation into the ξ-filtered expansion (43) via

$$\langle \xi : (\sigma(\varepsilon_h) - \sigma(\varepsilon))\rangle_Q = \left\langle \xi : \int_0^1 \left[\mathbb{A}(\cdot, \varepsilon + s(\varepsilon_h - \varepsilon)) - \mathbb{A}(\cdot, \varepsilon)\right] : (\varepsilon_h - \varepsilon)\, ds\right\rangle_Q , \tag{45}$$

we end up with the following improvement

$$\begin{aligned} \overline{\xi} : \overline{\sigma}_h(\overline{\varepsilon}) - \overline{\xi} : \overline{\sigma}(\overline{\varepsilon}) &= \langle (\xi - \xi_h) : (\sigma(\varepsilon) - \sigma(\varepsilon_h))\rangle_Q \\ &\quad + \left\langle \xi : \int_0^1 \left[\mathbb{A}(\cdot, \varepsilon + s(\varepsilon_h - \varepsilon)) - \mathbb{A}(\cdot, \varepsilon)\right] : (\varepsilon_h - \varepsilon)\, ds\right\rangle_Q . \end{aligned} \tag{46}$$

of Equation (42). The Cauchy–Schwarz inequality and the Lipschitz continuity (12) imply the estimate

$$\begin{aligned} \left|\overline{\xi} : \overline{\sigma}_h(\overline{\varepsilon}) - \overline{\xi} : \overline{\sigma}(\overline{\varepsilon})\right| &\le \alpha_+ \|\xi - \xi_h\|_{L^2} \|\varepsilon - \varepsilon_h\|_{L^2} \\ &\quad + \left\| \int_0^1 \left[\mathbb{A}(\cdot, \varepsilon + s(\varepsilon_h - \varepsilon)) - \mathbb{A}(\cdot, \varepsilon)\right]^T \xi\, ds \right\|_{L^2} \|\varepsilon - \varepsilon_h\|_{L^2} \\ &\le \frac{\alpha_+^2}{\alpha_-} \|v - P_h v\|_{H_0^1} \|u - P_h u\|_{H_0^1} \\ &\quad + \frac{\alpha_+}{\alpha_-} \left\| \int_0^1 \left[\mathbb{A}(\cdot, \varepsilon + s(\varepsilon_h - \varepsilon)) - \mathbb{A}(\cdot, \varepsilon)\right]^T \xi\, ds \right\|_{L^2} \|u - P_h u\|_{H_0^1}, \end{aligned} \tag{47}$$

where we used the a priori estimate (24) and the definition (36) of the field ξ_h. This estimate has a few direct implications

1. If the algorithmic tangent $\mathbb{A}$ is independent of ε, the second term (47) vanishes. Thus, we obtain the estimate

$$\left|\overline{\xi} : \overline{\sigma}_h(\overline{\varepsilon}) - \overline{\xi} : \overline{\sigma}(\overline{\varepsilon})\right| \leq \frac{\alpha_+^2}{\alpha_-} \|v - P_h v\|_{H_0^1} \|u - P_h u\|_{H_0^1}. \tag{48}$$

In particular, for the asymptotic behaviors

$$\|u - P_h u\|_{H_0^1} = O(h^p) \quad \text{and} \quad \|v - P_h v\|_{H_0^1} = O(h^p), \tag{49}$$

we deduce the convergence behavior

$$\left|\overline{\xi} : \overline{\sigma}_h(\overline{\varepsilon}) - \overline{\xi} : \overline{\sigma}(\overline{\varepsilon})\right| = O(h^{2p}). \tag{50}$$

Thus, we recover the result (32) reported by Ye-Chung,[14] theorem 5 for linear elasticity. Moreover, as a result of using nonenergetic arguments, our particular result includes affine-linear constitutive behavior, for example, linear thermoelasticity and linear viscoelasticity. The Li-Nirenberg estimates[42] are applicable in this case, as well, and $p = 1/2$ holds in the estimates (49) and (50) under appropriate regularity conditions on the data.

2. Due to the estimate

$$\left\| \int_0^1 \left[\mathbb{A}(\cdot, \varepsilon + s(\varepsilon_h - \varepsilon)) - \mathbb{A}(\cdot, \varepsilon)\right]^T : \xi \, ds \right\|_{L^2} \leq 2 \, \alpha_+ \, \|\xi\|_{L^2}, \tag{51}$$

and the assumed continuity of the algorithmic tangent $\mathbb{A}$ in the second variable, Lebesgue's dominated convergence theorem implies

$$\left\| \int_0^1 \left[\mathbb{A}(\cdot, \varepsilon + s(\varepsilon_h - \varepsilon)) - \mathbb{A}(\cdot, \varepsilon)\right]^T : \xi \, ds \right\|_{L^2} \to 0 \quad \text{as} \quad \|\varepsilon - \varepsilon_h\|_{L^2} \to 0. \tag{52}$$

Thus, under the asymptotic conditions (49), we obtain the result

$$\left|\overline{\xi} : \overline{\sigma}_h(\overline{\varepsilon}) - \overline{\xi} : \overline{\sigma}(\overline{\varepsilon})\right| = o(h^p). \tag{53}$$

As a consequence, the effective stresses do in fact converge faster than predicted by the conservative estimate (30), even in this rather general case.

The purpose of the estimate (53) was to state that some kind of superconvergence is expected, even under minimal hypotheses. From the point of view of numerical analysis it would be interesting to study whether the estimate (53) is sharp, that is, by exposing suitable examples, or to improve the estimate via more sophisticated techniques.

3. With the help of the Lipschitz condition (6) on the algorithmic tangent, we observe

$$\begin{aligned} \left\| \int_0^1 \left[\mathbb{A}(\cdot, \varepsilon + s(\varepsilon_h - \varepsilon)) - \mathbb{A}(\cdot, \varepsilon)\right]^T : \xi \, ds \right\|_{L^2} &\leq \int_0^1 \left\| \left[\mathbb{A}(\cdot, \varepsilon + s(\varepsilon_h - \varepsilon)) - \mathbb{A}(\cdot, \varepsilon)\right]^T : \xi \right\|_{L^2} ds \\ &\leq \|\xi\|_{L^\infty} \int_0^1 \left\| \left[\mathbb{A}(\cdot, \varepsilon + s(\varepsilon_h - \varepsilon)) - \mathbb{A}(\cdot, \varepsilon)\right]^T \right\|_{L^2} ds \\ &\leq \|\xi\|_{L^\infty} \int_0^1 Ms \, \|\varepsilon_h - \varepsilon\|_{L^2} \, ds \\ &= \frac{M}{2} \, \|\xi\|_{L^\infty} \, \|\varepsilon_h - \varepsilon\|_{L^2}, \end{aligned} \tag{54}$$

using Hölder's inequality. Thus, inequality (47) becomes

$$\left|\overline{\xi} : \overline{\sigma}_h(\overline{\varepsilon}) - \overline{\xi} : \overline{\sigma}(\overline{\varepsilon})\right| \leq \frac{\alpha_+^2}{\alpha_-} \|v - P_h v\|_{H_0^1} \|u - P_h u\|_{H_0^1} + \frac{M \, \alpha_+^2}{2 \, \alpha_-^2} \|\xi\|_{L^\infty} \|u - P_h u\|_{H_0^1}^2. \tag{55}$$

Thus, we may draw similar conclusions as in item 1. provided the linearized corrector ξ, defined via Equation (36), is essentially bounded. This is true under suitable hypotheses on the coefficient field $\mathbb{A}(\cdot, \varepsilon)$, see Li-Nirenberg,[42]

proposition 1.4. Please notice that the Li-Nirenberg result deals with linear elastic problems, possibly with eigenstrains, only. Thus, it is only applicable to the linearized corrector.

We wish to stress that we are not aware of a general result leading to a bounded linearized corrector field ξ. Thus, the boundedness of the field ξ may be treated as an additional assumption, as previously announced.

4. We restricted to the (fully integrated) Galerkin setting to clearly expose the ideas. Indeed, for linear elasticity, the quadratic rate estimate (32) follows from Galerkin orthogonality, and is, thus, essentially a consequence of the Pythagorean theorem.

   For the nonlinear case, this kind of route is blocked, and an alternative had to be found. Our strategy relied on finding an appropriate bilinear quantity which expresses the difference between the exact and the approximated effective stress tensor up to an explicit error term. The leading contribution could be shown to vanish by choosing the field ξ appropriately.

   Although fully integrated elements can be handled, nonconforming discretizations are the most popular in FFT-based computational homogenization[44] for performance reasons. Analyzing their convergence behavior requires handling the consistency error, and requires additional arguments. Unfortunately, we are not aware of a general argument akin to estimate (32) in the underintegrated setting extending the analysis of Bellis et al.[15] for laminates, even for the linear elastic case.
5. For inelastic materials, we are not aware of a general reference which provides the convergence rates

$$\|u - P_h u\|_{H^1_0} = O(h^{1/2}) \quad \text{and} \quad \|v - P_h v\|_{H^1_0} = O(h^{1/2}), \tag{56}$$

   observed empirically in computational experiments, see Section 3. There is a deeper mathematical reason for this shortcoming. In contrast to scalar elliptic equations, the regularity theory of elliptic systems (i.e., with vector-valued unknown) is less good-natured. To be more precise, both scalar and vector-valued elliptic systems share the higher regularity theory, but the partial regularity properties of solutions are in stark contrast. Higher regularity entails estimates for weak solutions of elliptic systems in Sobolev spaces under the requirement that the solution is essentially bounded. Partial regularity concerns deriving such a boundedness statement, typically in a Hölder norm, for weak solutions that are merely in a natural Sobolev space. For scalar (uniformly) elliptic equations, the celebrated results of De Georgi[45] and Nash[46] cover partial regularity for rough coefficients. In contrast, for elliptic systems, explicit counterexamples to partial regularity are known (in dimension 3 and higher). We refer to Giaquinta,[47] chapter II, for background and discussion.

   With this knowledge in mind, the results of Li-Nirenberg[42] are even more remarkable. Unfortunately, we are not aware of extensions of the Li-Nirenberg results to general nonlinear elastic models at small strains. Therefore, we consider the estimates (49) with rates $p = 1/2$ as empirical.
6. If only an approximate solution $\tilde{\varepsilon}_h$ of the corrector equation (21) is available, the following estimate

$$\begin{aligned}\left|\overline{\xi} : \langle \sigma(\tilde{\varepsilon}_h)\rangle_Q - \overline{\xi} : \overline{\sigma}(\overline{\varepsilon})\right| &\leq \alpha_+ \|\xi - \xi_h\|_{L^2} \|\varepsilon - \tilde{\varepsilon}_h\|_{L^2} + \left|\langle v_h \cdot \operatorname{div}\ \sigma(\tilde{\varepsilon}_h)\rangle_Q\right| \\ &\quad + \left\| \int_0^1 \left[\mathbb{A}(\cdot, \varepsilon + s(\tilde{\varepsilon}_h - \varepsilon)) - \mathbb{A}(\cdot, \varepsilon)\right]^T \xi \, ds \right\|_{L^2} \|\varepsilon - \tilde{\varepsilon}_h\|_{L^2} \end{aligned}, \tag{57}$$

   may be readily established in place of inequality (47). Thus, solving the corrector equation (21) to high accuracy is necessary to exploit superconvergence of the effective stresses.

   Please note that computational experiments[15] for linear elastic composites report that the effective stresses only converge linearly during iterative schemes, whereas the effective energy shows a quadratic convergence behavior. The caveat here is that these results use volume averaging to estimate the effective stresses, whereas *energy equivalence* has to be used to obtain a quadratic convergence behavior, see Schneider.[37]

3 | COMPUTATIONAL INVESTIGATIONS

3.1 | Setup

In this section, we would like to investigate the convergence rate of both the local stress and strain fields as well as the effective stresses upon grid refinement. More precisely, we investigate discretizations on regular (periodic) grids that

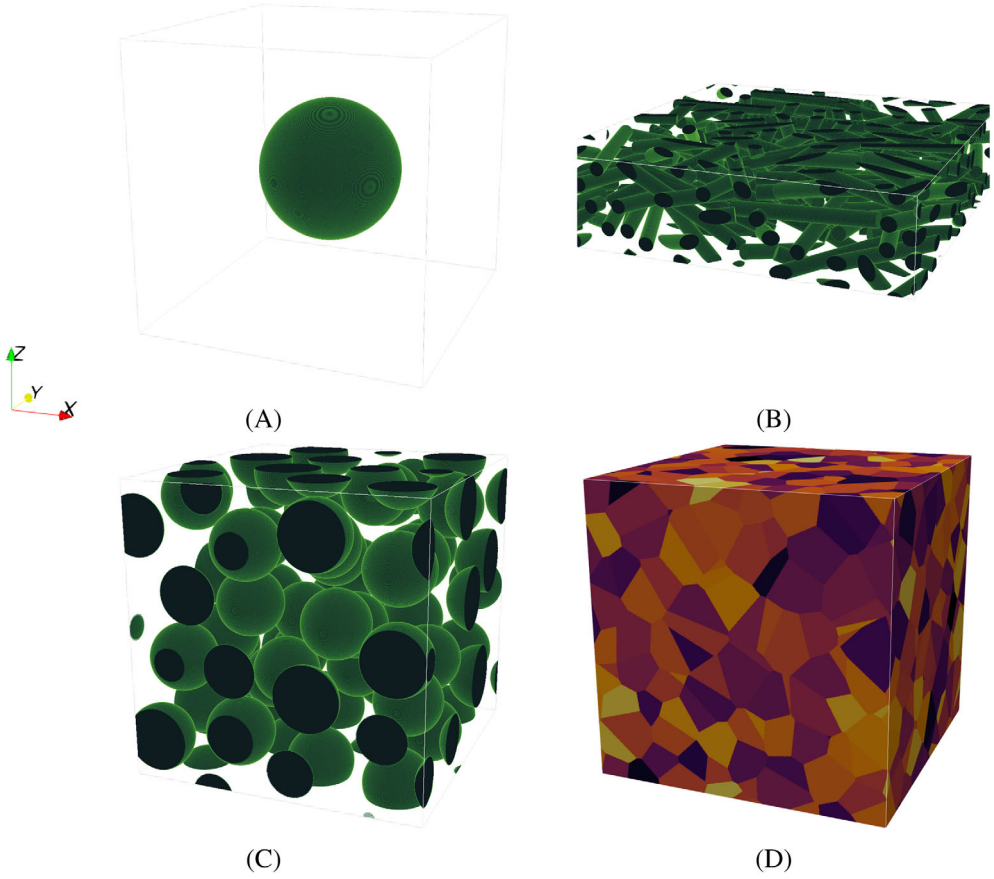

FIGURE 1 Microstructures considered in this article. (A) Single spherical inclusion; (B) Planar short-fiber composite; (C) Metal-matrix composite; (D) Polycrystalline microstructure

are amenable to FFT-based computational micromechanics.[44] As our reference, we consider the Moulinec–Suquet discretization,[7,48] which may be interpreted as an underintegrated Fourier–Galerkin discretization.[49,50] However, we will also consider alternative discretizations in Section 3.2. For elastic material behavior and for microstructures without pores, different computational experiments[13,21,51] revealed that the convergence rates of the different used discretizations are the same and only differ by the prefactor.

The experiments were run with an in-house FFT-based computational homogenization code.[52] For every level of discretization, the corrector equation (16) was solved to an accuracy of 10^{-5} using the convergence criterion described in Schneider,[44] section 3.6. Then, the effective stresses were computed by volume averaging.

We used a workstation with two AMD EPYC 7642 with 48 physical cores each as our hardware. The investigated microstructures are shown in Figure 1, and the subsequent sections provide details on the microstructures, also including both the constitutive models and the material parameters.

3.2 | Spherical inclusion

As our first example, we consider a rather simple microstructure with only a single spherical inclusion placed at the center of the microstructure, with a volume fraction of 6.54%. We consider resolutions N^3 with $N = 8, 16, \ldots, 1024$. At the highest resolution, the microstructure is shown in Figure 1A.

We furnish the inclusion with the material parameters of E-glass, whereas the matrix is governed by J_2-elastoplasticity with exponential-linear hardening

$$\sigma_0(\varepsilon_{\mathrm{eq}}) = \sigma_{\mathrm{Y}} + k_1\, \varepsilon_{\mathrm{eq}} + k_2(1 - \exp(-m\, \varepsilon_{\mathrm{eq}})). \tag{58}$$

TABLE 1 Material parameters for the short glass fiber reinforced polyamide, see Doghri et al.[53]

Fibers	$E = 72$ GPa	$\nu = 0.22$			
Matrix	$E = 2.1$ GPa	$\nu = 0.3$	$\sigma_Y = 29$ MPa, $k_1 = 139$ MPa	$k_2 = 32.7$ MPa	$m = 319.4$

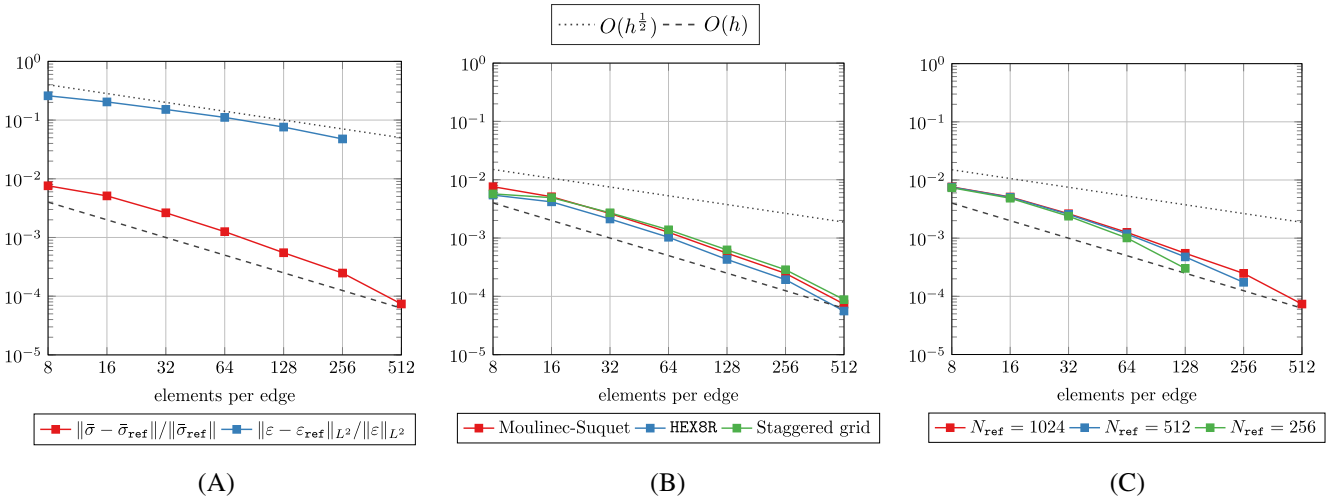

FIGURE 2 Relative error and convergence rates for a single load step and the spherical inclusion, see Figure 1A. (A) Relative error of effective stress and of local strain field; (B) Relative error of effective stress for different discretizations; (C) Influence of the edge resolution N_{ref} on effective-stress error

Thus, after an implicit discretization in time and in view of the pseudo-elastic setting,[38,39] which is standard in computational mechanics, the considered material model satisfies the prerequities required by the theory in Section 2.1. Indeed, due to the exponential-linear hardening (58), the statically condensed stress function (2) is strongly monotone and Lipschitz continuous. Moreover, the interface between the spherical inclusion and the matrix is smooth, and the Li-Nirenberg estimates[42] apply, at least for linear elasticity. Let us again emphasize that the theory developed in Section 2 only covers the Galerkin setting, whereas our computational investigations deal with a nonconforming setting, which is not covered by the theory.

The employed material parameters are summarized in Table 1. As our first setup, we consider 5% shear strain in the 2-3-plane, that is, $\varepsilon_{23} = 5\%$, applied in a *single* load step. The results are summarized in Figure 2. For a start, we investigate the relative error in the effective stress and in the local strain field, measured in the L^2-norm, see Figure 2A. The computation on the 1024^3-structure serves as our reference, that is, the ground truth. We observe that the local strain error is more than one magnitude larger than the error in the effective stress. For the finest discretization, the difference amounts to about two orders of magnitude. Moreover, the local strain error in L^2 closely follows the rate $h^{1/2}$, where h is the voxel size. In contrast, the effective stresses converge with the rate h, that is, with the quadratic rate of the local strain error. Thus, these investigations suggest that the theory presented in Section 2 is not restricted to the Galerkin setting, but holds for suitable underintegrated discretizations, as well.

To increase the confidence in our results, we investigate possible sources of error or deviation to some extent. In Figure 2B, we considered the discretization on a rotated staggered grid,[54,55] introduced into the FFT-based community by Willot[56] and identified as an underintegrated hexahedral trilinear finite element,[21] and the discretization on a staggered grid,[13] a finite-volume discretization that is particularly robust for porous microstructures.[40]

We observe that the three considered discretizations do not differ significantly in terms of the predicted effective stresses for the considered resolutions. Indeed, the differences are about an order of magnitude smaller than the relative errors.

Moreover, we consider the influence of the considered ground truth, that is, the reference resolution, in Figure 2C. Relative to a edge-length element-count N_{ref}, we observe that the relative errors are comparable if $N < N_{\mathrm{ref}}/2$, that is, only the result for $N = N_{\mathrm{ref}}/2$ should be considered with care.

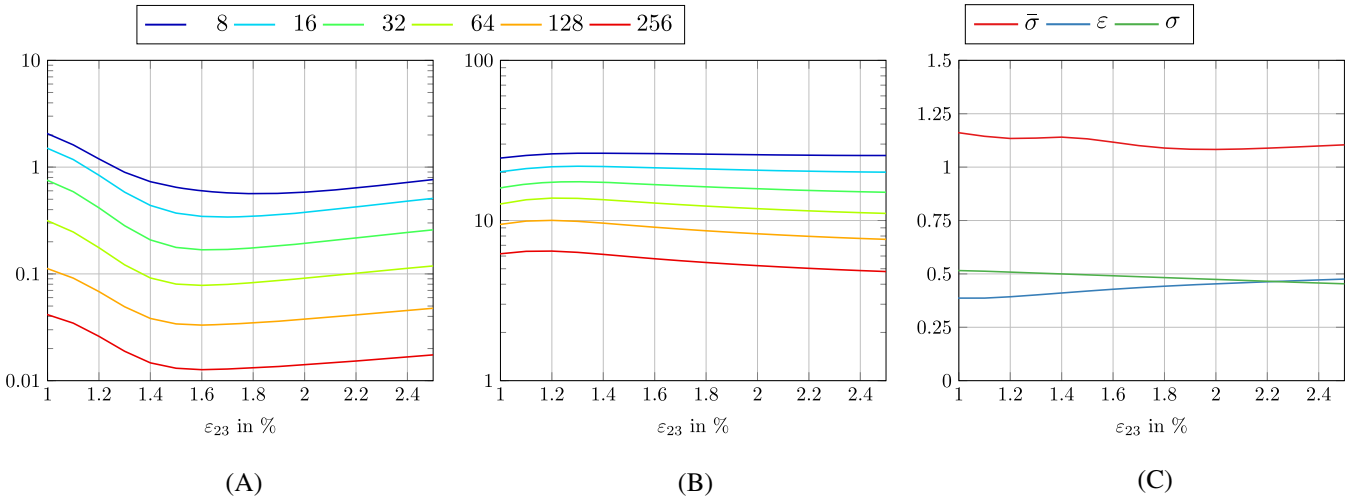

FIGURE 3 Relative error and convergence rates for 25 load steps and the spherical inclusion, see Figure 1A. (A) $\|\overline{\sigma} - \overline{\sigma}_{\text{ref}}\|/\|\overline{\sigma}_{\text{ref}}\|$ in %; (B) $\|\varepsilon - \varepsilon_{\text{ref}}\|_{L^2}/\|\varepsilon\|_{L^2}$ in %; (C) Convergence-rate exponents

After investigating a single load step, we move on to consider a scenario with *multiple* load steps. More precisely, we retain both the microstructure and the material models/parameters, but impose the 5% shear strain in 25 equidistant load steps. The results are recorded in Figure 3, where the microstructure with 512^3 voxels serves as the reference. Figure 3A shows the relative error in the effective stress as a function of the applied strain. We observe a decrease of this relative error up to 1.5% shear loading, consistently at every resolution. For higher loading, the errors are increasing again, but remain strictly below the levels reached in the initial elastic step.

Considering the local strain error in Figure 3B, we observe that the error level is about an order of magnitude larger than the relative error of the effective stress. Moreover, we observe that this error remains approximately constant throughout the deformation history.

We complement these investigations with estimates on the convergence rates, see Figure 3C, obtained by a linear regression of the respective curves in log-space. Please keep in mind that for this kind of computational experiment, slight over- and underestimations may not be excluded due to the low number of measurements. This is, however, a result of limited computational resource, in particular for nonlinear constitutive laws. We observe that both the local stress and stress errors converge with a rate of roughly $h^{1/2}$ for throughout the deformation history. In contrast, the effective stress converges at a higher rate, that is, h.

3.3 | Planar glass-fiber reinforced polyamide

After the initial, rather simple, example we turn our attention to more complex microstructures. We retain the material models and parameters of the previous section, but investigate a short-fiber reinforced microstructure. More precisely, we consider a structure reinforced by 20% E-glass fibers with an aspect ratio of 10 and a second-order fiber-orientation tensor[57,58]

$$A = \texttt{diag}(0.45, 0.45, 0.1), \tag{59}$$

that describes a slight deviation from a planar isotropic fiber-orientation state. As the fibers are described by cylinders, the interface between matrix and inclusions does not satisfy the $C^{1,\alpha}$-condition required for the Li-Nirenberg estimates,[42] in contrast to the spherical inclusion considered in Section 3.2.

The microstructure with dimensions $256 \times 256 \times 64$ μm^3, shown in Figure 1B, contains 106 fibers and was generated by the SAM[59] algorithm and the exact closure approximation.[60]

We consider resolutions $N \times N \times N/4$ with N in the range 64,128, … , 1024. We apply 1.5% shear strain in the 1-2-plane, that is, in the fiber plane, distributed over 30 equidistant load steps. The computation with $N = 1024$ serves as

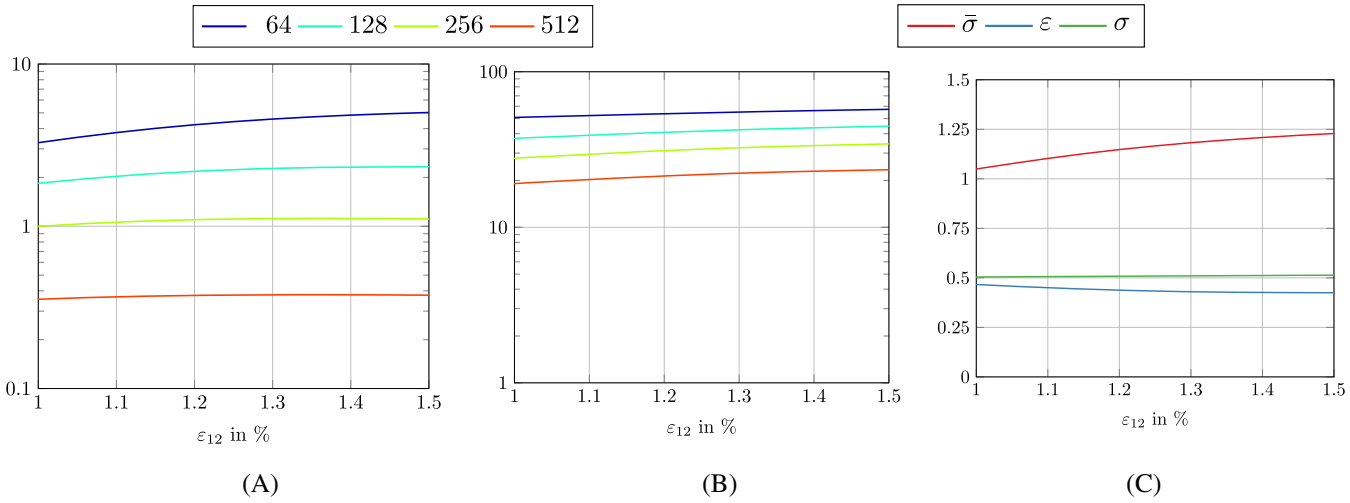

FIGURE 4 Relative error and convergence rates for 30 load steps and the planar glass-fiber reinforced polyamide, see Figure 1B. (A) $\|\bar{\sigma} - \bar{\sigma}_{\text{ref}}\|/\|\bar{\sigma}_{\text{ref}}\|$ in %; (B) $\|\varepsilon - \varepsilon_{\text{ref}}\|_{L^2}/\|\varepsilon\|_{L^2}$ in %; (C) Convergence-rate exponents

our the ground truth. Figure 4A shows the evolution of the relative effective-stress errors. For the coarse resolutions, the errors increase with increasing loading. For the two finest discretizations, this kind of error remains constant throughout the deformation. Thus, in contrast to the simple spherical inclusions, we do not observe a decrease of the error upon loading. However, such a scenario might happen for much finer resolutions which appear beyond reach of industrial-scale microstructures.

For the two finest discretizations, the effective stresses are approximated with a fidelity of 1%. However, the local strain fields, see Figure 4B, come with an error that exceeds 20%. We will take a closer look at this phenomenon later.

To close up the discussion, we investigate the convergence rates in Figure 4C. We notice that the local strains and stresses converge with a rate $h^{1/2}$, whereas the effective stresses converge (at least as fast as) as h.

With these investigations at hand, we take a closer look at the local fields. Figure 5 shows the local von-Mises equivalent strain fields in a special region at the final load step. At first glance, the different resolutions give rise to qualitatively similar local fields where high strains are observed around the fiber tips and between close fibers. Indeed for resolutions beyond 256^3, the difference to the reference field may appear rather small to the naked eye. However, the naked eye is a bit misled here as the strain levels are thresholded at 5% strain. Taking a look at the *local* relative error, we observe rather high errors around the fibers. Indeed, the error level exceeds 50%, and does not significantly decrease upon mesh refinement. Rather, the width of the error zone is decreasing, leading to a decrease of the L^2 error, but not the *maximum* error. Such a behavior does not come unexpected for the Moulinec–Suquet discretization,[7,48] as it is prone to the well-known ringing artifacts characteristic for Fourier-type discretizations. Please keep in mind that other popular discretizations in FFT-based computational micromechanics, see Schneider[24] for a recent overview, are also characterized by high errors at interfaces, essentially due to the jagged interfaces resulting from voxel discretizations.

The accuracy of the effective stresses, however, is not impaired by these high errors of the local fields due to favorable cancellations upon averaging.

3.4 | Metal matrix composite

We wish to investigate whether the results obtained for polyamide with E-glass reinforcements remain valid for different classes of composites. Therefore, we study a metal-matrix composite, that is, an aluminum alloy reinforced with stiff ceramic particles. More precisely, we consider a microstructure with 50 spherical inclusions of identical radius, filling 30% of the microstructure volume, see Figure 1C. For the generation procedure, we relied on the mechanical contraction method of Williams–Philipse.[61]

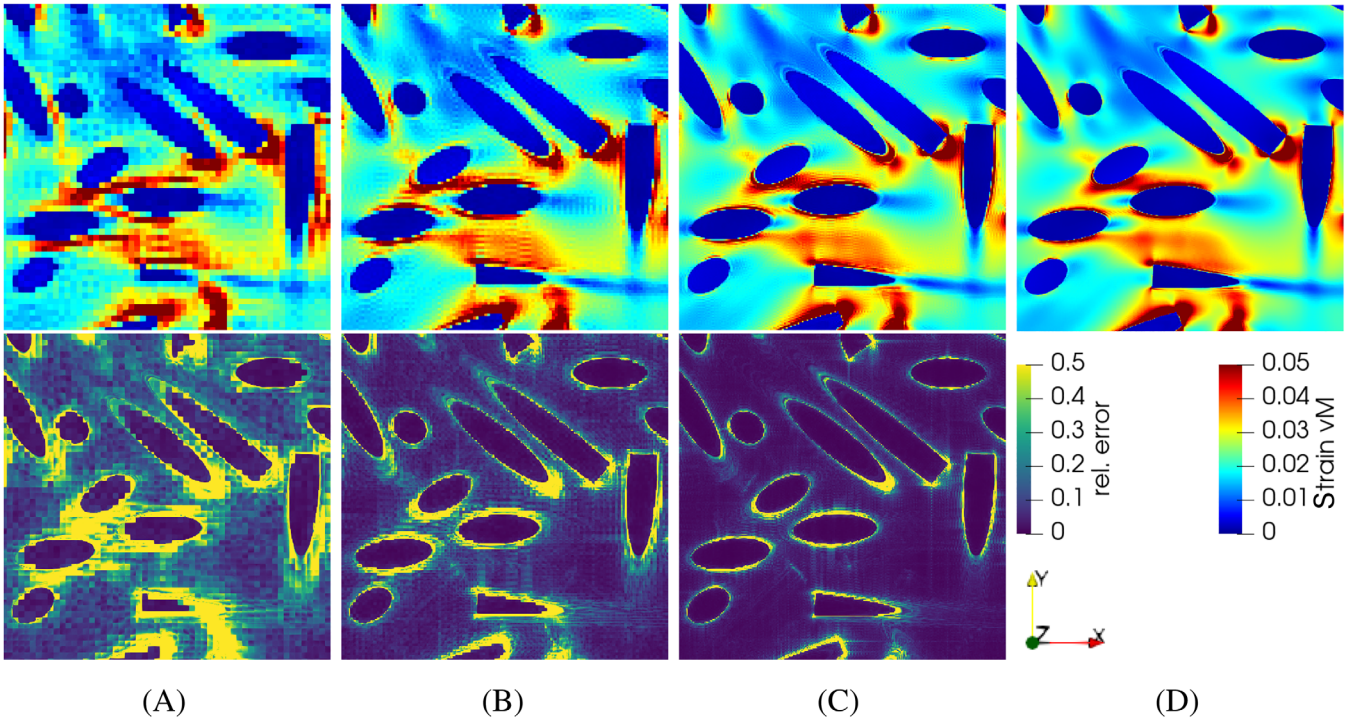

FIGURE 5 Close-up of the local von-Mises equivalent strain and the relative strain error $\|\varepsilon - \varepsilon_{\mathrm{ref}}\|/\|\varepsilon\|$ in the final load step for the planar glass-fiber reinforced polyamide, see Figure 1B. (A) 128^3; (B) 256^3; (C) 512^3; (D) 1024^3

TABLE 2 Material parameters for the metal-matrix composite, see Segurado et al.[62]

Inclusions	$E = 400$ GPa	$\nu = 0.2$		
Matrix	$E = 75$ GPa	$\nu = 0.3$	$\sigma_Y = 75$ MPa, $k = 416$ MPa	$m = 0.3895$

The ceramic particles are assumed to behave as an isotropic linear elastic medium, and the aluminum matrix follows a J_2 elastoplastic model with power-law hardening

$$\sigma_0(\varepsilon_{\mathrm{eq}}) = \sigma_{\mathrm{Y}} + k\, \varepsilon_{\mathrm{eq}}^m. \tag{60}$$

After an implicit Euler discretization in time, the statically condensed stress function (2) is Lipschitz continuous, but merely strictly monotone, as a consequence of the power-law hardening (60).

The material parameters[62] are summarized in Table 2. We consider resolutions N^3 with $N = 16, 32, \ldots, 512$, and the computation with $N = 512$ serves as our reference. The microstructured material is loaded to a shear strain ε_{23} of 0.5% in 40 equidistant load steps. The results are summarized in Figure 6. Upon plastification, the relative errors in the effective stresses increase consistently, see Figure 6A. More precisely, the relative error increases almost by an order of magnitude. In particular, resolutions which provide a high fidelity for the elastic predictions, that is, $N = 64$, may not be sufficiently accurate in the nonlinear regime.

Such conclusions may also be drawn when investigating the relative errors of the local strain field, see Figure 6B. As for the previously studied microstructures, the overall error level of the local strains is significantly higher than for the effective properties.

Taking a closer look at the convergence rates, shown in Figure 6C, we observe that the local stress and strain fields converge with a rate that is close to $h^{1/2}$. More precisely, the local strain fields converge at a slightly slower rate, whereas the stresses enjoy a slightly higher convergence rate. This behavior may be a consequence of the power-law hardening (60), as such a constitutive model fosters high strains, yet moderate increases in stress. Moreover, it appears as if this slightly higher rate of convergence is also reflected in the effective stresses. Indeed, the convergence-rate exponents for the effective stresses are roughly twice as high as their local counterparts, and increase up to almost 1.5.

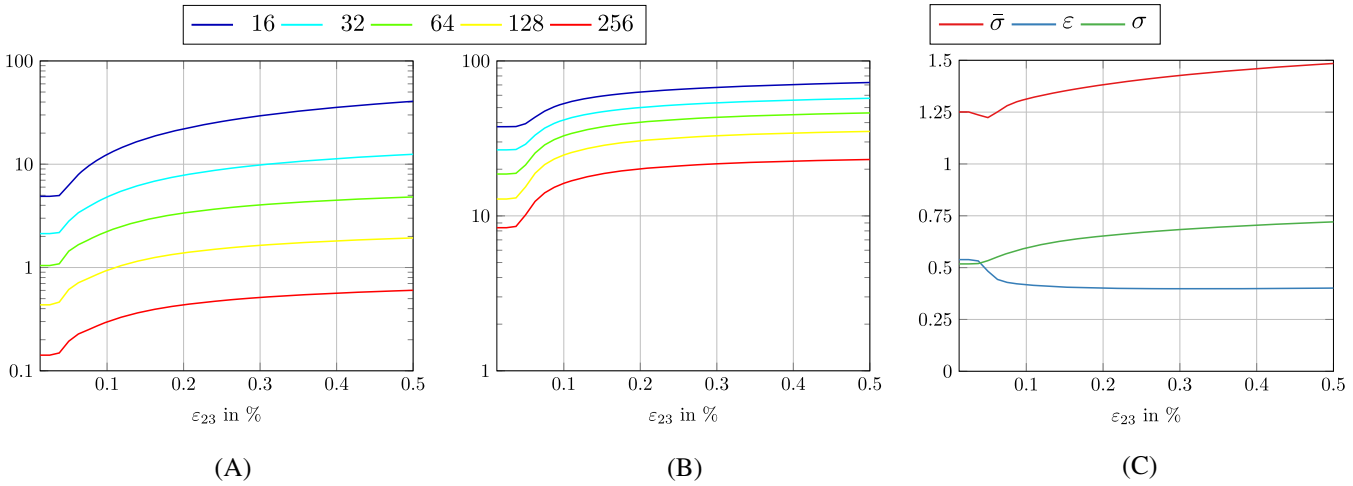

FIGURE 6 Relative error and convergence rates for 40 load steps and the metal-matrix composite, see Figure 1C. (A) $\|\overline{\sigma} - \overline{\sigma}_{\text{ref}}\|/\|\overline{\sigma}_{\text{ref}}\|$ in %; (B) $\|\varepsilon - \varepsilon_{\text{ref}}\|_{L^2}/\|\varepsilon\|_{L^2}$ in %; (C) Convergence-rate exponents

To sum up, we observe a slightly higher convergence rate for the stresses and a slightly slower convergence rate for the strains.

3.5 | Copper polycrystal

Last but not least, we consider an oxygen-free high thermal conductivity (OFHC) copper. The microstructure, shown in Figure 1D, consists of 512 grains of equal volume and was generated by a Laguerre tessellation whose grain volumes may be optimized in terms of a convex program.[63,64] Subsequently, the individual grains were furnished with crystal orientations constituting an isotropic orientation state, see Kuhn et al.[65] for a precise description of the method employed.

The material follows a single-crystal elastoviscoplastic model with the Hutchinson flow rule

$$\dot{\gamma}_\alpha = \dot{\gamma}_0 \operatorname{sgn}(\tau_\alpha) \left| \frac{\tau_\alpha}{\tau^{\text{F}}} \right|^n, \tag{61}$$

for the plastic slip γ_α in the αth slip system and a linear-exponential hardening in terms of the accumulated plastic slip

$$\tau^{\text{F}} = \tau_0 + (\tau_\infty - \tau_0) \left(1 - \exp\left(-\frac{\Theta_0 - \Theta_\infty}{\tau_\infty - \tau_0} \gamma \right) \right) + \Theta_\infty \gamma. \tag{62}$$

We refer to Wicht et al.[66] for more background on the model, whose statically condensed stress function (2) is Lipschitz continuous but not monotone. The elastic moduli correspond to OFHC copper at room temperature following Simmons-Wang.[67] The elastoviscoplastic parameters originate from Eghtesad et al.[68] The used material parameters are listed in Table 3. Please note that the algorithmic tangent (5) of the investigated material is not symmetric, adding further interest in this study.

We consider resolutions N^3 with $N = 16, 32, \ldots, 512$, and the highest resolution serves as the reference. The polycrystalline material is loaded to a shear strain ε_{23} of 0.5% in 25 equidistant load steps. The results are summarized in Figure 7. The relative errors of the effective stresses, see Figure 7A, increase slightly after the onset of plastification. However, they stabilize for more than 0.1% applied strain. Moreover, the overall level of the error is rather low. Even for the coarsest resolution of 16^3 voxels, the relative errors do not exceed 1%.

This degree of fidelity is not shared by the local strain fields, see Figure 7B. Even for the finest considered resolution, these errors exceed 10%. However, these errors do not significantly increase during loading, but remain on the same level.

A look at the convergence-rate exponents, see Figure 7C, reveals that both the local strain and stress fields converge with a rate $h^{1/2}$ rather precisely. The effective stresses show a higher rate of convergence, that is, an empirical $h^{3/2}$ relationship.

TABLE 3 Material parameters for the polycrystalline microstructure[67,68]

Cubic stiffness	$C_{11} = 170.2$ GPa	$C_{12} = 114.9$ GPa	$C_{44} = 61.0$ GPa
Flow rule	$\dot{\gamma}_0 = 0.001\text{s}^{-1}$	$n = 20$	
Hardening	$\Theta_0 = 250$ MPa	$\Theta_\infty = 14$ MPa	$\tau_\infty = 113.5$ MPa
Yield stress	$\tau_0 = 14.5$ MPa		
Lattice type	FCC		
Slip systems	$\{111\}\langle 110\rangle$.		

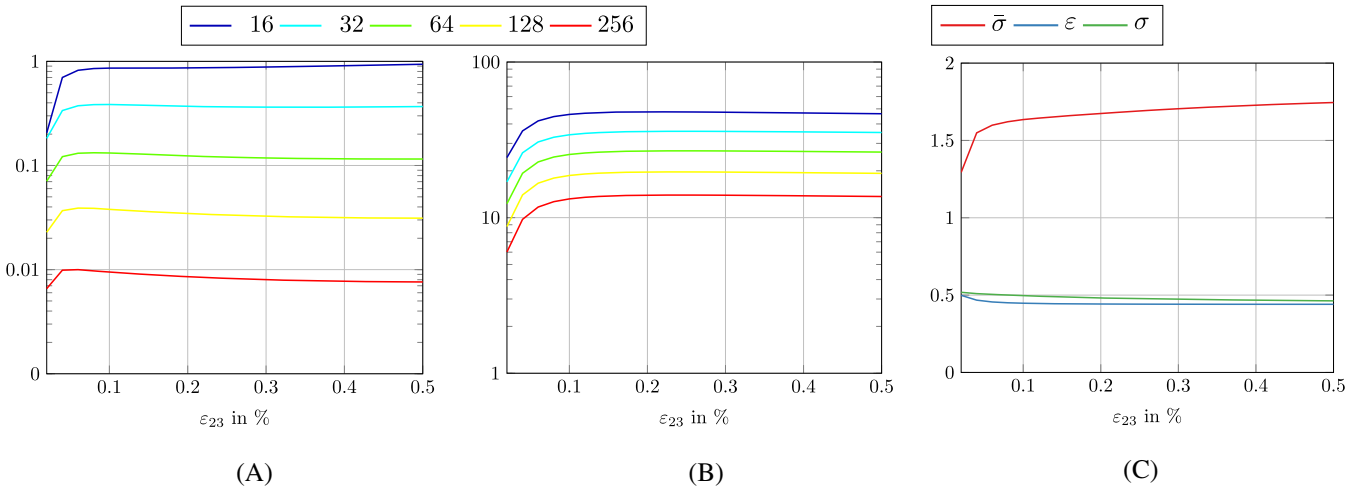

FIGURE 7 Relative error and convergence rates for 25 load steps and the polycrystalline microstructure, see Figure 1D. (A) $\|\bar{\sigma} - \bar{\sigma}_{\text{ref}}\|/\|\bar{\sigma}_{\text{ref}}\|$ in %; (B) $\|\varepsilon - \varepsilon_{\text{ref}}\|_{L^2}/\|\varepsilon\|_{L^2}$ in %; (C) Convergence-rate exponents

These investigations thus may shed light on the effectiveness of regular grid type methods for computational crystal plasticity.[69,70] In particular, the results demonstrate that the required resolution depends strongly on the purpose of the computation. For instance, in concurrent multiscale simulations[71] where the effective stress is of interest, only a few voxels per grain are sufficient, whereas investigations of local fields routinely operate on microstructures resolved by several thousand voxels per grain.[72-74]

4 | CONCLUSION

This work was concerned with the question whether the effective Cauchy stress in the computational homogenization of inelastic material models converges faster than the local fields. Computational experiments in the isothermal, quasistatic and small-strain setting with popular FFT-based computational homogenization methods indicate that the L^2-error of both the local strain and stress fields converge as the square root of the voxel edge-length h, whereas the effective stresses converge linearly in h. Moreover, we provided theoretical arguments for this superconvergence in case of Galerkin discretizations based on a close inspection of the macroscopic stress power. Unfortunately, there is still a gap between the theoretical results and the computational experiments, as underintegrated discretizations are typically favored over (fully integrated) Galerkin schemes due to performance reasons. Further ideas are required to close this gap.

Both the computational experiments and the theoretical developments should increase the confidence that regular grid based methods may be safely used for inelastic homogenization. However, the results also indicate that caution has to be taken with quantities different from the effective stress (or energy). For instance, investigations on local fields should be considered with caution.

During the finalization of the article, we became aware that there appears still to be a lack of theoretical work on modern computational homogenization methods, for instance on explicit convergence rates for the trigonometric

discretization of Moulinec-Suquet.[7,48] Indeed, most of the work is concerned with the approximation of smooth functions[75] or does not provide explicit rates.[14,50] Yet, the discretization is used with confidence for almost three decades, indicating stable convergence with h of the effective properties for nonporous materials.

Similarly, convergence (without rate) of Willot's discretization[56] was established by Ye-Chung,[14] but explicit rates appear to be unknown. Possibly, the equivalence of the discretized systems corresponding to Willot's discretization on a rotated staggered grid and the nonconforming P_1-finite element[76,77] may be exploited.

It might also be of interest what happens for non-quadratic energies[78,79] or whether it is possible to utilize the theoretical framework to speed up computational schemes, as done in the linear elastic context.[37]

ACKNOWLEDGMENTS

Support by the Deutsche Forschungsgemeinschaft (DFG, German Research Foundation)–255730231—is gratefully acknowledged. M. Schneider received partial support from the European Research Council within the Horizon Europe program—project 101040238. We thank C. Bellis, F. Legoll, and F. Otto for stimulating discussions and the reviewers for helpful suggestions. Open Access funding enabled and organized by Projekt DEAL.

DATA AVAILABILITY STATEMENT

The data that support the findings of this study are available from the corresponding author upon reasonable request.

ORCID

Matti Schneider https://orcid.org/0000-0001-7017-3618

REFERENCES

1. Suquet PM. Elements of homogenization for inelastic solid mechanics. In: Sanchez-Palencia E, Zaoui A, eds. *Homogenization Techniques for Composite Media*. Springer; 1987:1157-1171.
2. Matouš K, Geers MGD, Kouznetsova VG, Gillman A. A review of predictive nonlinear theories for multiscale modeling of heterogeneous materials. *J Comput Phys*. 2017;330:192-220.
3. Guedes JM, Kikuchi N. Preprocessing and postprocessing for materials based on the homogenization method with adaptive finite element methods. *Comput Methods Appl Mech Eng*. 1990;83(2):143-198.
4. Bakhvalov NS, Knyazev AV. Fictitious domain methods and computation of homogenized properties of composites with a periodic structure of essentially different components. In: Marchuk GI, ed. *Numerical Methods and Applications*. CRC Press; 1994:221-276.
5. Kafafy R, Lin T, Lin Y, Wang J. Three-dimensional immersed finite element methods for electric field simulation in composite materials. *Int J Numer Methods Eng*. 2005;64:940-972.
6. Moës N, Cloirec M, Cartraud P, Remacle J-F. A computational approach to handle complex microstructure geometries. *Comput Methods Appl Mech Eng*. 2003;192(28–30):3163-3177.
7. Moulinec H, Suquet P. A fast numerical method for computing the linear and nonlinear mechanical properties of composites. *Compt Rend Acad Sci Sér II*. 1994;318(11):1417-1423.
8. Arbenz P, van Lenthe GH, Mennel U, Müller R, Sala M. A scalable multi-level preconditioner for matrix-free μ-finite element analysis of human bone structures. *Int J Numer Methods Eng*. 2008;73(7):927-947.
9. Zhu Y, Sifakis E, Teran J, Brandt A. An efficient parallelizable multigrid framework for the simulation of elastic solids. *ACM Trans Graph*. 2010;29(2):1-18.
10. Chevalier Y, Pahr D, Allmer H, Charlebois M, Zysset PK. Validation of voxel-based FE method for prediction of the uniaxial apparent modulus of human trabecular bone using macroscopic mechanical tests and nanoindentation. *J Biomech*. 2007;40:3333-3340.
11. Pahr D, Zysset PK. A comparison of enhanced continuum FE with micro FE models of human vertebral bodies. *J Biomech*. 2009;42:455-462.
12. Zangmeister T, Andrä H, Müller R. Comparison of XFEM and Voxelbased FEM for the approximation of discontinuous stress and strain at material interfaces. *Tech Mech*. 2013;33(2):131-141.
13. Schneider M, Ospald F, Kabel M. Computational homogenization of elasticity on a staggered grid. *Int J Numer Methods Eng*. 2016;105(9):693-720.
14. Ye C, Chung ET. Numerical analysis of several FFT-based schemes for computational homogenization. arXiv preprint arXiv:2201.01916; 2022.
15. Bellis C, Moulinec H, Suquet P. Eigendecomposition-based convergence analysis of the Neumann series for laminated composites and discretization error estimation. *Int J Numer Methods Eng*. 2020;121:201-232.
16. Köbler J, Magino N, Andrä H, Welschinger F, Müller R, Schneider M. A computational multi-scale model for the stiffness degradation of short-fiber reinforced plastics subjected to fatigue loading. *Comput Methods Appl Mech Eng*. 2021;373:113522.
17. Magino N, Köbler J, Andrä H, Welschinger F, Müller R, Schneider M. A multiscale high-cycle fatigue-damage model for the stiffness degradation of fiber-reinforced materials based on a mixed variational framework. *Comput Methods Appl Mech Eng*. 2022;388:114198.
18. Magino N, Köbler J, Andrä H, Welschinger F, Müller R, Schneider M. A space-time upscaling technique for modeling high-cycle fatigue-damage of short-fiber reinforced composites. *Compos Sci Technol*. 2022;222:109340.

19. Hill R. Elastic properties of reinforced solids: some theoretical principles. *J Mech Phys Solids*. 1963;11(5):357-372.
20. Mandel J. *Plasticité classique et viscoplasticité: CISM-1971*. Springer; 1972.
21. Schneider M, Merkert D, Kabel M. FFT-based homogenization for microstructures discretized by linear hexahedral elements. *Int J Numer Methods Eng*. 2017;109:1461-1489.
22. Leuschner M, Fritzen F. Fourier-accelerated nodal solvers (FANS) for homogenization problems. *Comput Mech*. 2018;62:359-392.
23. Ladecký M, Leute RJ, Falsafi A, et al. Optimal FFT-accelerated finite element solver for homogenization. arXiv:2203.02962, 2022.
24. Schneider M. Voxel-based finite elements with hourglass control in FFT-based computational homogenization. *Int J Numer Methods Eng*. 2022;2022:1-32.
25. Křižek M, Neittaanmäki P. Superconvergence phenomenon in the finite element method arising from averaging gradients. *Numer Math*. 1984;45:105-116.
26. Andreev AB, Lazarov RD. Superconvergence of the gradient for quadratic triangular finite elements. *Numer Methods PDEs*. 1988;4:15-32.
27. Goodsell G, Whiteman JR. A unified treatment of superconvergent recovered gradient functions for piecewise linear finite element approximations. *Int J Numer Methods Eng*. 1989;27:469-481.
28. Zienkiewicz OC, Zhu JZ. The superconvergence patch-recovery (SPR) and adaptive finite element refinement. *Comput Methods Appl Mech Eng*. 1992;101:207-224.
29. Babuška I, Strouboulis T, Upadhyay CS, Gangaraj SK. Validation of recipes for the recovery of stresses and derivatives by a computer-based approach. *Math Comput Model*. 1994;20(6):45-89.
30. Babuška I, Strouboulis T, Upadhyay CS, Gangaraj SK. Computer-based proof of the existence of superconvergence points in the finite element method; superconvergence of the derivatives in finite element solutions of Laplace's, Poisson's and the elasticity equations. *Numer Methods PDEs*. 1996;12:347-392.
31. Garcia Archilla B, Novo J, Titi ES. Postprocessing the Galerkin method: a novel approach to approximate inertial manifolds. *SIAM J Numer Anal*. 1998;35:941-972.
32. Garcia Archilla B, Novo J, Titi ES. An approximate inertial manifolds approach to postprocessing the Galerkin method for the Navier-Stokes equations. *Math Comput*. 1999;68(227):893-911.
33. Garcia Archilla B, Novo J, Titi ES. Postprocessing the Galerkin method: the finite element case. *SIAM J Numer Anal*. 2000;37:470-499.
34. Xu J. Two-grid discretization techniques for linear and nonlinear PDEs. *SIAM J Numer Anal*. 1996;33(5):1759-1777.
35. Schatz AH, Sloan IH, Wahlbin LB. Superconvergence in finite element methods and meshes that are locally symmetric with respect to a point. *SIAM J Numer Anal*. 1996;33:505-521.
36. Laing CR, McRobie A, Thompson JMT. The post-processed Galerkin method applied to nonlinear shell vibrations. *Dyn Stab Syst*. 1999;14(2):163-181.
37. Schneider M. Superaccurate effective elastic moduli via postprocessing in computational homogenization. *Int J Numer Methods Eng*. 2022;123(17):4119-4135.
38. Ortiz L, Stainier L. The variational formulation of viscoplastic constitutive updates. *Comput Methods Appl Mech Eng*. 1999;171: 419-444.
39. Miehe C. Strain-driven homogenization of inelastic microstructures and composites based on an incremental variational formulation. *Int J Numer Methods Eng*. 2002;55:1285-1322.
40. Schneider M. Lippmann-Schwinger solvers for the computational homogenization of materials with pores. *Int J Numer Methods Eng*. 2020;121(22):5017-5041.
41. Renardy M, Rogers RC. *An Introduction to Partial Differential Equations*. Springer; 2004.
42. Li Y, Nirenberg L. Estimates for elliptic systems from composite material. *Commun Pure Appl Math*. 2003;56(7):892-925.
43. Mazzucato AL, Nistor V. Well-posedness and regularity for the elasticity equation with mixed boundary conditions on polyhedral domains and domains with cracks. *Arch Ration Mech Anal*. 2010;195:25-73.
44. Schneider M. A review of non-linear FFT-based computational homogenization methods. *Acta Mech*. 2021;232:2051-2100.
45. De Giorgi E. Sulla differenziabilità e l'analiticità delle estremali degli integrali multipli regolari. Memorie della Accademia delle Scienze di Torino. Classe di Scienze Fisiche, Matematicahe e Naturali; Vol. 3, 1957:25-43.
46. Nash J. Parabolic equations. *Proc Natl Acad Sci*. 1957;43:754-758.
47. Giaquinta M. *Multiple Integrals in the Calculus of Variations and Nonlinear Elliptic Systems*. Princeton University Press; 1983.
48. Moulinec H, Suquet P. A numerical method for computing the overall response of nonlinear composites with complex microstructure. *Comput Methods Appl Mech Eng*. 1998;157:69-94.
49. Vondřejc J, Zeman J, Marek I. An FFT-based Galerkin method for homogenization of periodic media. *Comput Math Appl*. 2014;68(3):156-173.
50. Schneider M. Convergence of FFT-based homogenization for strongly heterogeneous media. *Math Meth Appl Sci*. 2015;38(13):2761-2778.
51. Kabel M, Merkert D, Schneider M. Use of composite voxels in FFT-based homogenization. *Comput Methods Appl Mech Eng*. 2015;294:168-188.
52. Schneider M. On the Barzilai-Borwein basic scheme in FFT-based computational homogenization. *Int J Numer Methods Eng*. 2019;118(8):482-494.
53. Doghri I, Brassart L, Adam L, Gérard J-S. A second-moment incremental formulation for the mean-field homogenization of elasto-plastic composites. *Int J Plast*. 2011;27(3):352-371.
54. Saenger EH, Gold N, Shapiro SA. Modeling the propagation of elastic waves using a modified finite-difference grid. *Wave Motion*. 2000;31:77-92.

55. Saenger EH, Bohlen T. Finite-difference modeling of viscoelastic and anisotropic wave propagation using the rotated staggered grid. *Geophysics*. 2004;69:583-591.
56. Willot F. Fourier-based schemes for computing the mechanical response of composites with accurate local fields. *Comp Rend Méce*. 2015;343:232-245.
57. Kanatani K. Distribution of directional data and fabric tensors. *Int J Eng Sci*. 1984;22:149-164.
58. Advani SG, Tucker CL. The use of tensors to describe and predict fiber orientation in short fiber composites. *J Rheol*. 1987;31:751-784.
59. Schneider M. The Sequential Addition and Migration method to generate representative volume elements for the homogenization of short fiber reinforced plastics. *Comput Mech*. 2017;59:247-263.
60. Montgomery-Smith S, He W, Jack D, Smith D. Exact tensor closures for the three-dimensional Jeffery's equation. *J Fluid Mech*. 2011;680:321-335.
61. Williams S, Philipse A. Random packings of spheres and spherocylinders simulated by mechanical contraction. *Phys Rev E*. 2003;67(5):1-9.
62. Segurado J, Llorca J, González C. On the accuracy of mean-field approaches to simulate the plastic deformation of composites. *Scr Mater*. 2002;46(7):525-529.
63. Kitagawa J, Mérigot Q, Thibert B. Convergence of a Newton algorithm for semi-discrete optimal transport. *J Eur Math Soc*. 2019;21(9):2603-2651.
64. Kuhn J, Schneider M, Sonnweber-Ribic P, Böhlke T. Fast methods for computing centroidal Laguerre tessellations for prescribed volume fractions with applications to microstructure generation of polycrystalline materials. *Comput Methods Appl Mech Eng*. 2020;369:113175.
65. Kuhn J, Schneider M, Sonnweber-Ribic P, Böhlke T. Generating polycrystalline microstructures with prescribed texture coefficients. *Comput Mech*. 2022;70:639-659.
66. Wicht D, Schneider M, Böhlke T. An efficient solution scheme for small-strain crystal-elasto-viscoplasticity in a dual framework. *Comput Methods Appl Mech Eng*. 2020;358:112611.
67. Simmons G, Wang H. *Single Crystal Elastic Constants and Calculated Aggregate Properties: A Handbook*. MIT Press; 1971.
68. Eghtesad A, Barrett TJ, Germaschewski K, Lebensohn RA, McCabe RJ, Knezevic M. OpenMP and MPI implementations of an elasto-viscoplastic fast Fourier transform-based micromechanical solver for fast crystal plasticity modeling. *Adv Eng Softw*. 2018;126:46-60.
69. Segurado J, Lebensohn RA, Lorca JL. Computational homogenization of polycrystals. *Adv Appl Mech*. 2018;51:1-114.
70. Lebensohn RA, Rollett AD. Spectral methods for full-field micromechanical modelling of polycrystalline material. *Comput Mater Sci*. 2020;173:109336.
71. Kochmann J, Wulfinghoff S, Ehle L, Mayer J, Svendsen B, Reese S. Efficient and accurate two-scale FE-FFT-based prediction of the effective material behavior of elasto-viscoplastic polycrystals. *Comput Mech*. 2018;61:751-764.
72. Rollett AD, Lebensohn RA, Groeber M, Choi Y, Li J, Rohrer GS. Stress hot spots in viscoplastic deformation of polycrystals. *Model Simul Mater Sci Eng*. 2010;18(7):074005.
73. Lim H, Battaile CC, Bishop JE, Foulk JW III. Investigating mesh sensitivity and polycrystalline RVEs in crystal plasticity finite element simulations. *Int J Plast*. 2019;121:101-115.
74. Gallardo-Basile F-J, Naunheim Y, Roters F, Diehl M. Lath martensite microstructure modeling: a high-resolution crystal plasticity simulation study. *Dent Mater*. 2021;14(3):691.
75. Zygmund A. *Trigonometric Series*. Vol I. Cambridge University Press; 1990.
76. Park C, Sheen D. P1-nonconforming quadrilateral finite element methods for second-order elliptic problems. *SIAM J Numer Anal*. 2003;41(2):624-640.
77. Ye C, Chung ET, "P_1 nonconforming quadrilateral finite element space with periodic boundary conditions: Part I. fundamental results on dimensions, bases, solvers, and error analysis. arXiv preprints, Vol. 2201.10658, 2022:1-26.
78. Schneider M. An FFT-based method for computing weighted minimal surfaces in microstructures with applications to the computational homogenization of brittle fracture. *Int J Numer Methods Eng*. 2020;121(7):1367-1387.
79. Ernesti F, Schneider M. A fast Fourier transform based method for computing the effective crack energy of a heterogeneous material on a combinatorially consistent grid. *Int J Numer Methods Eng*. 2021;122(21):6283-6307.

How to cite this article: Schneider M, Wicht D. Superconvergence of the effective Cauchy stress in computational homogenization of inelastic materials. *Int J Numer Methods Eng*. 2022;1-20. doi: 10.1002/nme.7149